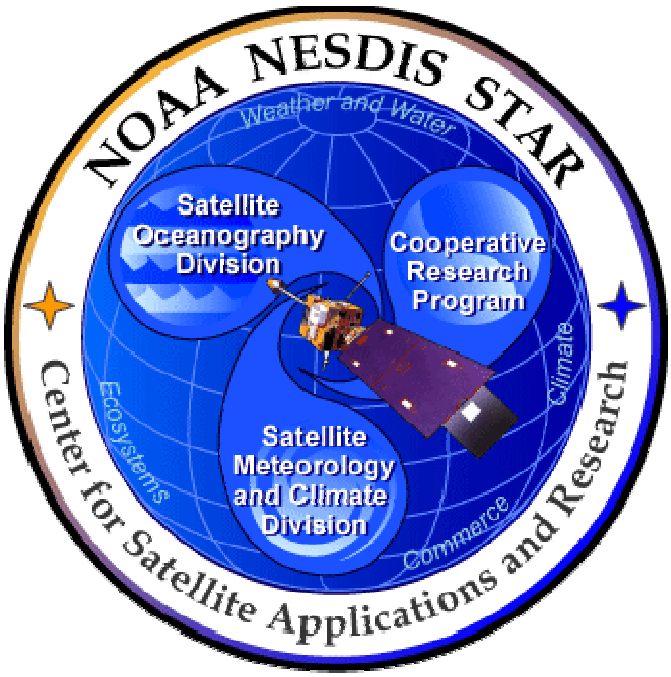

NOAA NESDIS
CENTER for SATELLITE APPLICATIONS and RESEARCH

ALGORITHM THEORETICAL BASIS DOCUMENT

ABI Earth Radiation Budget
Upward Longwave Radiation: Surface (ULR)

Hai-Tien Lee[(1)], Istvan Laszlo[(2)] and Arnold Gruber[(1)]

[(1)]CICS/ESSIC-NOAA/UMCP
[(2)]NOAA/NESDIS/STAR, AOSC/UMCP

Version 2.0
September 24, 2010

TABLE OF CONTENTS

LIST OF FIGURES

LIST OF TABLES

LIST OF ACRONYMS

ABI	Advanced Baseline Imager
ASTER	Advanced Space-borne Thermal Emission and Reflection Radiometer
ATBD	Algorithm Theoretical Basis Document
AWG	Algorithm Working Group
CERES	The Cloud and the Earth's Radiant Energy System
COVE	CERES Ocean Validation Experiment\
CRTM	Community Radiative Transfer Model
DLR	Downward Longwave Radiation at Surface
DLW	Downward Longwave Radiation at Surface
GFS	Global Forecast Model
GSIP	GOES Surface Insolation Product
JHU	Johns Hopkins University
LST	Land skin temperature
PIR	Eppley Precision Infrared Radiometer
SST	Sea surface temperature
SURFRAD	NOAA Surface Radiation Budget Network
ULR	Upward Longwave Radiation at Surface
ULW	Upward Longwave Radiation at Surface

ABSTRACT

This Algorithm Theoretical Basis Document (ATBD) describes the physical and mathematical basis of the algorithm developed to retrieve the ***Upward Longwave Radiation: Surface (ULR)*** by the Advanced Baseline Imager (ABI) onboard the geostationary satellite GOES-R. The ULR is the total upward thermal radiative flux density emitted by the earth surface in the unit of watt per square meter. It is one of the four radiative fluxes that determine the earth surface radiation budget. The other three components are the downward longwave radiation, the incoming solar radiation and the reflected solar radiation. The ULR retrieval is performed for clear-sky condition only due to the limitations of the ABI land skin temperature and sea surface temperature retrievals under cloudy sky. Algorithm evaluation was conducted with the surrogate data and ground truth observations. It is shown that this algorithm could meet the F&PS requirements.

1 INTRODUCTION

1.1 Purpose of This Document

The Earth Radiation Budget (ERB) Surface Upward Longwave Radiation (ULR) algorithm theoretical basis document (ATBD) provides a high level description of and the physical basis for the estimation technique of longwave radiative flux at the top of the atmosphere with images taken by the Advanced Baseline Imager (ABI) flown on the GOES-R series of NOAA geostationary meteorological satellites. The ULR is estimated with the ABI retrieved surface temperature and an estimated broadband emissivity for each target.

1.2 Who Should Use This Document

The intended users of this document are those interested in understanding the physical basis of the algorithms and the error characteristics of this product. This document also provides information useful to anyone maintaining or modifying the original algorithm.

1.3 Inside Each Section

This document is broken down into the following main sections.

- **System Overview**: Provides relevant details of the ABI and provides a brief description of the product generated by the algorithm.

- **Algorithm Description**: Provides all the detailed description of the algorithm including its physical basis, its input and output.

- **Assumptions and Limitations**: Provides an overview of the current limitations of the approach and gives the plan for overcoming these limitations with further algorithm development.

- **Validation**: Provides summaries of up to date validation results and descriptions of error characteristics.

1.4 Related Documents

This related documents include the specifications of the GOES-R Mission Requirements Document (MRD v3.0), Function and Performance Specification (F&PS) and the references given through out.

1.5 Revision History

Version 0.1 (Aug. 15, 2008)
The Version 0.1 ATBD draft accompanies the delivery of the Version 1 algorithm code package to the GOES-R AWG Algorithm Integration Team (AIT).

Version 1.0 (Sep. 26, 2009)
Version 1.0 describes the algorithm at the 80% F&PS requirement level, and accompanies the delivery of the Version 4 algorithm code package to the GOES-R AWG Algorithm Integration Team (AIT).

Version 2.0 (Sep. 5, 2010)
Version 2.0 describes the algorithm at the 100% F&PS requirement level, and accompanies the delivery of the Version 5 algorithm code package to the GOES-R AWG Algorithm Integration Team (AIT). Newly implemented features include the sea surface emissivity, the definitions of metadata, quality flags, and diagnostic output.

2 OBSERVING SYSTEM OVERVIEW

This section will describe the product generated by the ABI Surface Upward Longwave Radiation (ULR) and the requirements it places on the sensor.

2.1 Product Generated

The ULR algorithm is performed at each ABI pixel. In terms of the MRD, it is responsible as one of the surface Earth Radiation Budget components. The ULR is estimated directly from the ABI retrieved land/sea skin temperature under the clear sky condition. Additional information about the surface emissivity is provided as static ancillary data.

The balance of the following four radiation quantities determines the radiation budget at the earth's surface: the incoming and reflected solar radiative fluxes, and the downward and upward longwave radiative fluxes. The surface reflected solar radiative flux is a GOES-R baseline product. The radiative fluxes, the latent heat flux, and the sensible heat flux determine the surface energy balance that is important to the modeling of the surface property, e.g., in the land data assimilation.

The ULR algorithm is performed for all ABI pixels. In terms of the MRD, it is responsible as one of the Surface Earth Radiation Budget components. The ULR is calculated using the ABI retrieved parameters, including the skin temperature and the window emissivity with which the broadband emissivity is estimated. The ULR calculation can be performed for slant observations to within the local zenith angle limit of the skin temperature/emissivity retrievals.

2.2 Instrument Characteristics

The ABI channels relevant to the ULR retrievals are those used in the land skin temperature and sea surface temperature retrievals. Table 2-1 summarizes ABI instrument specifications and lists the ABI channels relevant to ULR derivation. The ABI ULR F&PS requirements are listed in Table 2-2.

Table 2-1. ABI channel numbers and wavelengths that are relevant to the ULR derivation.

Channel ID	*Wavelength Microns*	*Hor. Res.*	*Upper and lower 50% response points (in microns)*	*Noise @ Ref.*	*Max. Level*	*Used for DLR*
1	0.47	1km	0.45±0.01 - 0.49±0.01	300/1	100 %	
2	0.64	0.5km	0.59±0.01 - 0.69±0.01	300/1	100 %	
3	0.865	1km	0.8455±0.01 - 0.8845±0.01	300/1	100 %	
4	1.378	2km	1.3705±0.005 - 1.3855±0.005	300/1	100 %	
5	1.61	1km	1.58±0.01 - 1.64±0.01	300/1	100 %	
6	2.25	2km	2.225±0.01 - 2.275±0.01	300/1	100 %	
7	3.90	2km	3.80±0.05 - 4.00±0.05	0.1 K	400 K	
8	6.185	2km	5.77±0.03 - 6.6±0.03	0.1 K	300 K	
9	6.95	2km	6.75±0.03 - 7.15±0.03	0.1 K	300 K	
10	7.34	2km	7.24±0.02 - 7.44±0.02	0.1 K	320 K	
11	8.5	2km	8.3±0.03 - 8.7±0.03	0.1 K	330 K	✓
12	9.61	2km	9.42±0.02 - 9.8±0.03	0.1 K	300 K	
13	10.35	2km	10.1±0.1 - 10.6±0.1	0.1 K	330 K	✓
14	11.2	2km	10.8±0.1 - 11.6±0.1	0.1 K	330 K	✓
15	12.3	2km	11.8±0.1 - 12.8±0.1	0.1 K	330 K	✓
16	13.3	2km	13.0±0.06 - 13.6±0.06	0.3 K	305 K	

Table 2-2. F&PS requirements for the ABI ULR product.

Name	User & Priority	Geographic Coverage (G, H, C, M)	Vertical Resolution	Horizontal Resolution	Mapping Accuracy	Measurement Range	Measurement Accuracy	Refresh Rate/Coverage Time	VAGL
Upward Longwave Radiation: Surface	GOES-R	C	N/A	25 km	5 km	50-900 W/m^2	30 W/m^2	60 min	3236 sec
Upward Longwave Radiation: Surface	GOES-R	FD	N/A	100 km	5 km	50-900 W/m^2	30 W/m^2	60 min	3236 sec

Product Measurement Precision	Temporal Coverage Qualifiers	Product Extent Qualifier	Cloud Cover Conditions Qualifier	Product Statistics Qualifier
20 W/m^2	Day and Night	Quantitative out to at least 62 degrees LZA	Clear conditions associated with threshold accuracy	Over specified geographic area
20 W/m^2	Day and Night	Quantitative out to at least 62 degrees LZA	Clear conditions associated with threshold accuracy	Over specified geographic area

3 ALGORITHM DESCRIPTION

3.1 Algorithm Overview

The surface upward longwave radiation (ULR) is derived by the physical method using satellite retrievals for the inputs. The primary inputs include the skin temperature and surface broadband emissivity. The land skin temperature (LST) algorithm is defined by the AWG Land Team, while the sea surface temperature (SST) algorithm is defined by the AWG SST Team. The ABI-retrieved downward longwave radiation (DLW) is used to

account for reflected component of the upward longwave flux at the surface, combining with the surface broadband reflectivity information.

The ULR derivation is formulated as,

$$ULW = \varepsilon_{LW}(T) \cdot \sigma T^4 + R_{LW}(S) \cdot DLW \qquad (3.1)$$

ULR – surface upward longwave radiative flux density (Wm^{-2})
DLW – surface downward longwave radiative flux density (Wm^{-2})
ε_{LW} *– surface broadband emissivity (unit-less)*
R_{LW} *– surface broadband reflectivity (unit-less)*
σ – the Stefan-Boltzmann constant, 5.6704e-8 $Wm^{-2}K^{-4}$
T – skin temperature (°K)
S – state of the atmosphere (parameterized)

Eq. 3.1 assumes that the ULR can be estimated as the sum of the surface thermal emission plus the first-order reflected radiation of the downward longwave radiation. The surface broadband emissivity is a function of material type and surface temperature. The surface broadband reflectivity is dependent on the energy distribution of the downward longwave radiation spectrum, and therefore is denoted here as a function of the atmospheric state. In this implementation, we neglect the temperature dependence in the broadband emissivity, and assumed the surface as a grey body that is essentially equivalent to neglecting the differences in spectral distributions between the downward and upward thermal radiation. The development of these estimating parameters is described in the Section 3.4 Theoretical Description.

3.2 Processing Outline

The processing outline of the ULR is summarized in Fig. 3-1. This processing scheme is applied to each pixel.

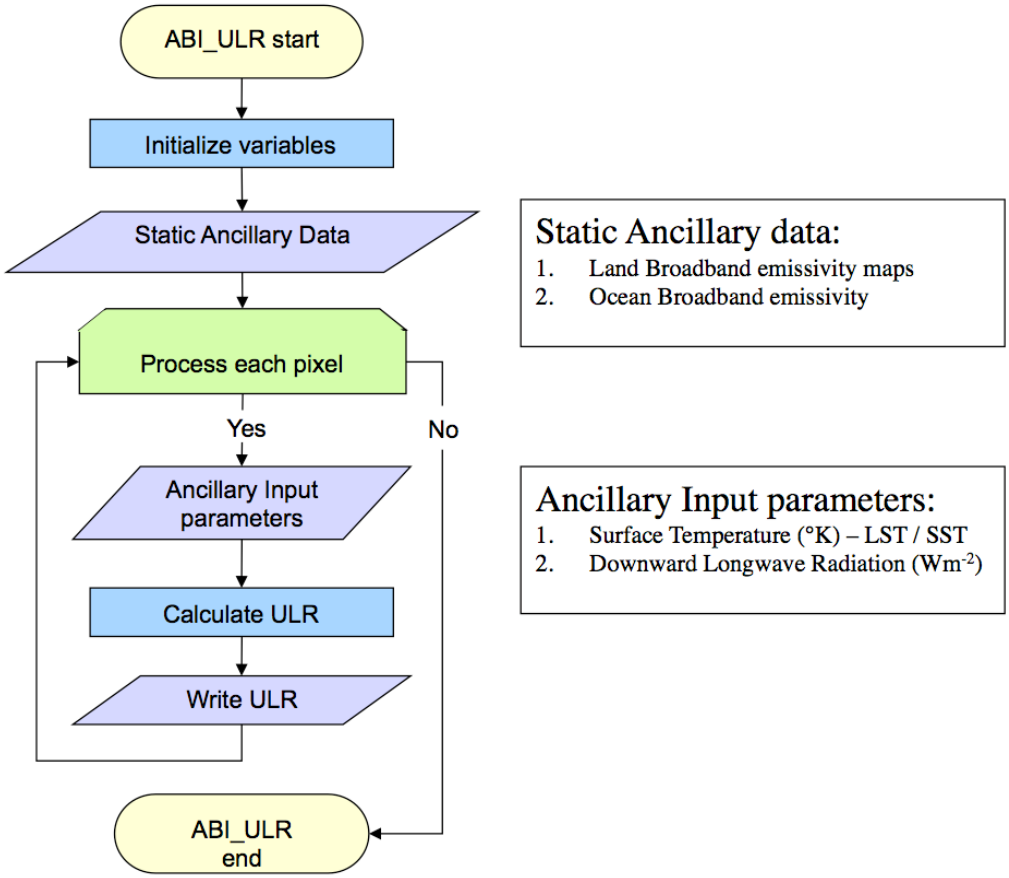

Figure 3-1 High Level Flowchart of the ABI ULR algorithm illustrating the main processing sections.

3.3 Algorithm Input

This section describes the input needed to process the ULR. The ULR derivation is for each pixel independent from the surrounding pixels.

3.3.1 Primary Sensor Data

The ULR algorithm does not use sensor radiance data directly. Table 3-1 lists the primary sensor inputs that will be used by ULR algorithm.

Table 3-1. ABI primary sensor input data used by the ULR algorithm.

Name	Type	Description	Dimension
Latitude	input	Center latitude	grid (xsize, ysize)
Longitude	input	Center longitude	grid (xsize, ysize)
View geometry	input	ABI local zenith angle	grid (xsize, ysize)
QC flags	input	ABI quality control flags with level 1b data	grid (xsize, ysize)

* Grid (xsize and ysize) are the output grid dimension that is product specific and is determined by the post processing.

3.3.2 Ancillary Data

The ULR algorithm currently uses a static broadband emissivity database. This can be improved by incorporating information from the ABI window emissivity retrieval when available. For current implementation, the ancillary data (Table 3-2) include:

- Monthly climatological broadband longwave emissivity derived from the SeeBor (Seemann et al., 2008) emissivity database. This is a static database.

Table 3-2. Ancillary input data used by the ULR algorithm.

Name	Type	Description	Dimension
Land Broadband Emissivity	input	Broadband Emissivity over land Database, monthly maps on 0.5°x0.5° resolution	Floating number: 720x360x12
Ocean Broadband Emissivity	input	Broadband Emissivity over ocean	Floating number

3.3.3 Derived Data

The ABI ULR is a physical algorithm that depends directly from the ABI-retrieved physical properties (Table 3-3) at the surface, including:

- Land skin temperature (LST)
- Sea surface temperature (SST)
- Downward longwave radiation at the surface (DLR)

Table 3-3. Land skin temperature, sea surface temperature, and downward longwave radiation at the surface.

Name	Type	Description	Dimension
Land skin temperature	input	ABI retrieved land skin temperature (LST)	Floating number
Sea surface temperature	input	ABI retrieved Sea surface temperature (SST)	Floating number
Downward longwave radiation at surface	input	ABI retrieved Downward longwave radiation at surface (DLR)	Floating number

3.4 Theoretical Description

The upward component of the surface longwave radiation includes the surface thermal emission plus the reflected portion of the downwelling longwave radiation reaching the surface. The transmission of longwave radiation through the land surface is usually negligible, but might not be so over the water. For simplicity, we have assumed zero transmissivity for both land and water surface here. The estimation of surface thermal emission requires the knowledge of the 'skin' temperature and an emissivity. The skin temperature is a radiative-equivalent thermal parameter corresponding to the thermal emission from the surface of a material with a given emissivity. The spectral emissivity is a function of wavelength and material. Theoretically it is not function of emitting temperature. The spectral reflectance measurements for a wide range of material and wavelength intervals are available through several studies, including the Johns Hopkins Spectral Library (Salisbury and D'Aria, 1992), SeeBor (Seemann et al., 2008), ASTER compilation database (http://speclib.jpl.nasa.gov).

Spectral emissivity retrieval from hyperspectral instruments covering wide spectral intervals is possible but not routinely produced (e.g., derived from AIRS or IASI). Narrowband emissivity retrieved from atmospheric window channels is routinely available, e.g., MODIS, and it might be generated by ABI as well. There were several

studies that use narrowband emissivity retrievals to estimate band-averaged emissivity, e.g., Ogawa *et al.* (2002), Wang *et al.,* (2005), and Jin and Liu (2006).

The present implementation of ULR algorithm assumes the earth surface as a grey body with a prescribed broadband emissivity. The possible sources of broadband emissivity for global application includes the climatology database created by the CERES Surface and Atmospheric Radiation Budget group (SARB), and the one derived from the SeeBor spectral emissivity database.

A possible improvement of the ABI upward longwave radiation accuracy is to estimate the broadband emissivity and reflectivity dynamically with the ABI window emissivity retrievals at the 8.6, 10.3, 11, and 12 μm channels. Since that a skin temperature will also be retrieved along with the window emissivity retrieval, as a byproduct (Jun Li, pers. comm., July 2008), one needs to be cautious about the possible inconsistency when using the window emissivity information together with the land team's skin temperature retrieval in ULR calculation.

The definition and derivation of the surface broadband emissivity and reflectivity is discussed in the following sections.

3.4.1 Physics of the Problem

Refer the respective ATBD for the Land Skin Temperature and Sea Surface Temperature for surface temperature retrievals.

The derivation methods of the broadband emissivity and reflectivity are described below.

3.4.2 Mathematics Description

Deriving Broadband Emissivity and Reflectivity

The spectral emissivity ε_ν is a function of material type and frequency, assuming isotropic emission. The laboratory measurements are available over a wide range of material type and frequency.

The band-averaged emissivity is defined as

$$\overline{\varepsilon_{\nu}} \equiv \frac{\int_{\nu} \varepsilon_\nu L_\nu \, d\nu}{\int_{\nu} L_\nu \, d\nu} \qquad (3.2)$$

where L_ν is the radiance, and ν is the frequency interval of interest.

The longwave broadband emissivity, denoted as ε_{LW}, is the band-averaged emissivity over the entire infrared frequency range. For practical calculation consideration, it is 0-3000 cm^{-1} for narrow-band model simulation purpose. Since the Planck function cannot be evaluated at 0 cm^{-1}, a small wavenumber, e.g., 25 cm^{-1}, is usually used for line-by-line model calculation.

It should be noted that the band-averaged emissivity is dependent on the spectral distribution of both the source radiation energy and the emissivity. Many applications neglect the dependency in energy distribution, nevertheless.

There are several emissivity approximations used in literatures that need to be clarified here.

1. The band-averaged emissivity is used to represent the thermal emission equivalent to a blackbody emission at brightness temperature *T* given the spectral emissivity. For a given spectral interval, the relationship is defined in Eq. 3.3. The ***broadband emissivity*** that corresponds to total infrared emission is determined according to the Stefan-Boltzmann's law as:

$$\varepsilon_{LW}(T) = \frac{\int_{LW} \varepsilon_\nu \pi B_\nu(T)\, d\nu}{\int_{LW} \pi B_\nu(T)\, d\nu} = \frac{\int_{LW} \varepsilon_\nu \pi B_\nu(T)\, d\nu}{\sigma T^4} \tag{3.3}$$

   where $B_\nu(z')$ is the Planck function evaluated at wave number ν with the temperature *T*, σ is the Stefan-Boltzmann constant.

2. Under grey body assumption, the emissivity is independent of frequency. We denote the ***grey body emissivity*** ε_{GB}. Assuming zero transmissivity, the reflectivity for grey body is:

$$R_{GB} = 1 - \varepsilon_{GB} \tag{3.4}$$

3. For surface radiation energy budget, there is another way of defining the effective emissivity: the emissivity that takes into account of the both effects of surface thermal emission and the reflection of the downward radiation reaching the surface. This definition is valid for spectral (Eq. 3.5) as well band-averaged property. The band averaging over the entire LW spectrum is defined in Eq. 3.6.

$$\varepsilon_\nu^{eff}(T) \equiv \frac{\varepsilon_\nu B_\nu(T) + (1-\varepsilon_\nu) F_\nu^{\downarrow}}{B_\nu(T)} \tag{3.5}$$

$$\begin{aligned} \varepsilon_{LW}^{eff}(T) &= \frac{\int_{LW} \pi \left(\varepsilon_\nu B_\nu(T) + (1-\varepsilon_\nu) F_\nu^{\downarrow} \right) d\nu}{\int_{LW} \pi B_\nu(T)\, d\nu} \\ &= \frac{\int_{LW} \pi \left(\varepsilon_\nu B_\nu(T) + (1-\varepsilon_\nu) F_\nu^{\downarrow} \right) d\nu}{\sigma T^4} \end{aligned} \tag{3.6}$$

   where $F_\nu^{\downarrow}$ is the downward spectral flux at the surface, σ is the Stefan-Boltzmann constant. The Planck function $B_\nu(T)$ describes the surface thermal emission at temperature *T*.

In the ABI ULR algorithm, we derive the broadband emissivity following Eq. 3.3 with prescribed spectral emissivity databases. Furthermore, we assume the surface acts as a grey body such that the reflectivity is estimated following Eq. 3.4.

Most of the laboratory measured LW emissivity databases do not extend into far infrared spectrum (for wavenumber smaller than about 600 cm^{-1}). The derivation of broadband emissivity is sensitivity to the assumptions how the extrapolation of emissivity for far infrared region was done due to the fact that the energy distribution is peaked around 500 to 600 cm^{-1} at typical surface temperatures. There are two ways to extrapolate the emissivity: a) assume emissivity of one, referred as '*blackbody extrapolation*'; b) use the last available emissivity measurement and extend it to the end of the spectrum, referred as '*constant extrapolation*'. The two assumptions can cause surface LW broadband emissivity to differ by up to 0.02.

Broadband Emissivity for Land

SeeBor baseline emissivity database was downloaded from CIMSS. The spatial resolution is also 0.05°x0.05° for wavelengths 3.6, 4.3, 5.0, 5.8, 7.6, 8.3, 9.3, 10.8, 12.1, and 14.3 μm. Following Eq. 3.3, and replacing the radiation source function to the Planck function for surface thermal emission, the broadband emissivity is,

$$\varepsilon_{LW}(T) = \frac{\int B_\nu(T)\varepsilon_\nu \, d\nu}{\int B_\nu(T) d\nu} \tag{3.7}$$

Fig. 3-2 shows an example of the derivation process of the broadband emissivity. The spectral emissivity is given at 699.3, 826.4, 925.9, 1075.2, 1204.8, 1315.7, 1724.1, 2000.0, 2325.5, 2702.7 cm-1 (black curve with asterisk marks); the Planck function at 300°K is shown in red (with normalized scale); and their convolution result is shown in blue. The extrapolation of the emissivity outside data range is assumed to stay on the value at the last point. The temperature dependence of the broadband emissivity is illustrated in Fig. 3-3. The 'constant extrapolation' is used for land surface types.

The SeeBor emissivity database has a original spatial resolution of 0.05 degrees, or about 5km. That gives a 7200x3600 grid map. For ULR implementation purpose, it is reduced to a 0.5 degrees resolution by averaging the spectral responses.

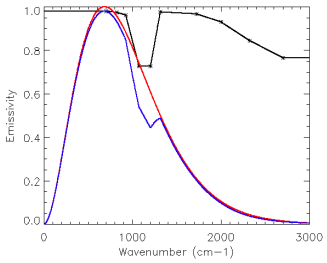

Figure 3-2 Example of the convolution of the spectral emissivity with the Planck function for the broadband emissivity derivation.

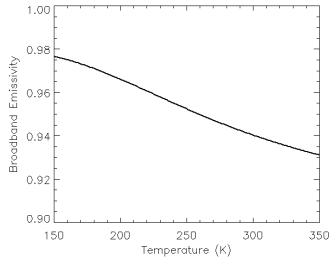

Figure 3-3 Example of the temperature dependence in the broadband emissivity for the same spectral emissivity use in Fig. 3-2.

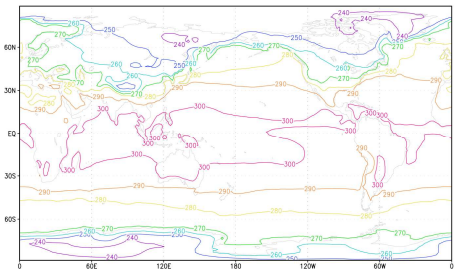

Figure 3-4 January surface temperature climatology obtained from the NCEP Reanalysis 2.

Surface temperature climatology is obtained from NCEP Reanalysis 2 1979-1988 monthly means. Fig. 3-4 is the January surface temperature climatology. NCEP Reanalysis 2 data is obtained from NOAA Operational Model Archive Distribution System (http://nomad3.ncep.noaa.gov as of Sept 25, 2008).

Monthly broadband emissivity climatology is derived with these corresponding climatological monthly mean surface temperatures. Fig. 3-5 shows the seasonal variation of the climatological broadband emissivity, at 0.5°x0.5° spatial resolution.

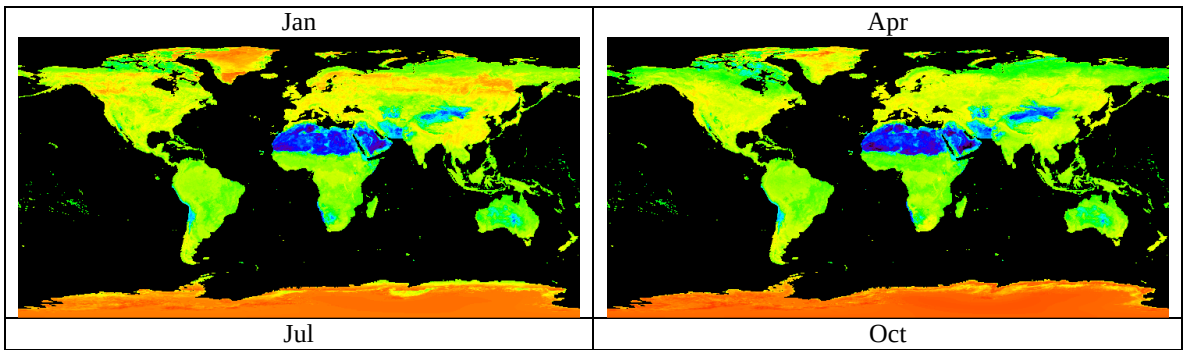

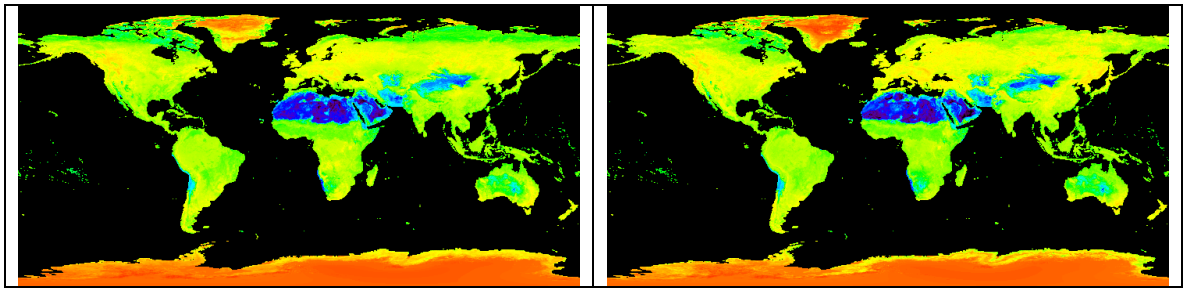

Figure 3-5 Seasonal variation of the broadband emissivity climatology determined with the SeeBor spectral emissivity and NCEP Reanalysis-2 surface temperature 1979-1988 climatology. The rainbow colors correspond to emissivity values ranged between 0.95 and 1.00.

Broadband Emissivity for Ocean (Seawater)

CERES SARB's Fu-Liou model requires band-averaged emissivity for its 12 bands. They have used the 'constant extrapolation' assumptions to derive the band averages. However, the broadband emissivity value 0.991 (see ATBD, Wilbur et al., 1999) was derived using 'black' assumption (but not documented). The 'black extrapolation' assumption is preferred for seawater due to the strong absorption by water vapor (David Kratz, pers comm).

The CRTM seawater emissivity v1.2 database (van Delst and Wu, 2000, see Fig. 3-6) is a function of the temperature *T*, the surface wind speed V, and the local zenith angle θ. It is shown to be very consistent with the Johns Hopkins University (JHU) seawater emissivity (see Fig. 3-7). The broadband seawater emissivity $\varepsilon_{Broadband}$, remains to be a function of local zenith angle, surface temperature and surface wind speed, is 0.986, 0.986, 0.982, and 0.957, for 0°, 20°, 40° and 60°, respectively, based on the CRTM database given a 288°K temperature and a 7.5 ms^{-1} wind speed.

$$\varepsilon_{Broadband}(T,V,\theta) = \frac{\int_{LW} \varepsilon_{\upsilon}(T,V,\theta) B_{\upsilon}(T)\, d\upsilon}{\int_{LW} B_{\upsilon}(T)\, d\upsilon} \qquad (3.8)$$

The seawater spectral emissivity has a relatively weak dependency on the wind speed. We chose to calculate the broadband emissivity at a wind speed of 7.5 ms^{-1}.

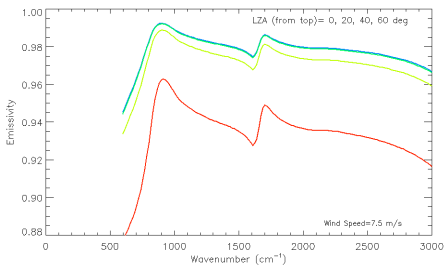

Figure 3-6 CRTM ver.1.2 Emissivity database. (van Delst and Wu, 2000).

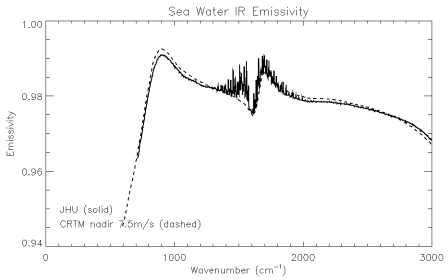

Figure 3-7 Comparison of CRTM ver.1.2 (at nadir) and JHU emissivity database.

CRTM ver.1.2 seawater emissivity (van Delst and Wu, 2000; Wu and Smith, 1997) is a function of frequency, local zenith angle, and wind speed. Figure 1 shows the dependence of emissivity in frequency and local zenith angle at a wind speed 7.5 m/s.

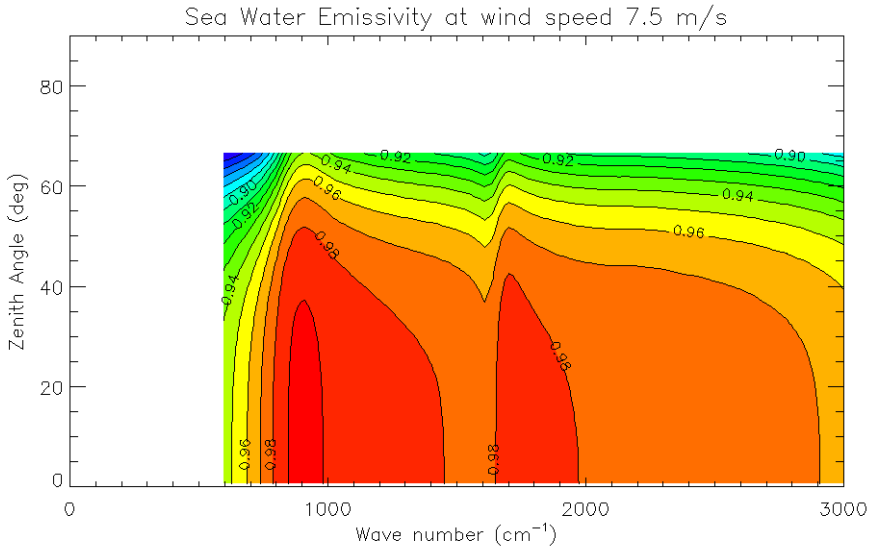

Fig. 1. Dependence of emissivity in frequency and local zenith angle at 7.5 m/s wind speed. Note the data is not available for wave numbers 0-595 cm^{-1} and local zenith angles 67-90 degrees.

The broadband emissivity for a non-Lambertian sea surface can be defined as,

$$\varepsilon_{LW}(T,V)=\frac{\int_0^{2\pi}\int_0^{\frac{\pi}{2}}\int_0^{\infty}\varepsilon_\nu(V,\theta)B_\nu(T)\cos\theta\sin\theta d\nu d\theta d\phi}{\int_0^{2\pi}\int_0^{\frac{\pi}{2}}\int_0^{\infty}B_\nu(T)\cos\theta\sin\theta d\nu d\theta d\phi}$$

Define the cosine-weighted hemispherical integral of spectral emissivity $\bar{\varepsilon}_\nu$ as (see Fig. 2),

$$\bar{\varepsilon}_\nu(V)=\frac{\int_0^{2\pi}\int_0^{\frac{\pi}{2}}\varepsilon_\nu(V,\theta)\cos\theta\sin\theta d\theta d\phi}{\int_0^{2\pi}\int_0^{\frac{\pi}{2}}\cos\theta\sin\theta d\theta d\phi}$$

Then, the seawater broadband emissivity ε_{LW}, remained to be a function of temperature and wind speed, can be written as (see Fig. 3),

$$\varepsilon_{LW}(T,V) = \frac{\int_0^\infty \bar{\varepsilon}_\nu(V) B_\nu(T) d\nu}{\int_0^\infty B_\nu(T) \mathrm{s} d\nu}$$

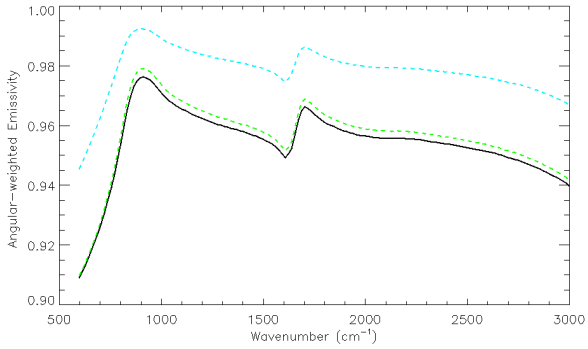

Fig. 2. Cosine-weighted seawater emissivity for the non-Lambertian sea surface (black solid curve) at wind speed 7.5 m/s. The CRTM emissivity at nadir (cyan dotted) and 53° (green dotted) are shown for reference.

We derive the seawater broadband emissivity ε_{LW} at temperature 288°K and wind speed 7.5 m/s for the ULR derivation over ocean purpose. The results are

$\varepsilon_{LW}(T = 288°K, V = 7.5 ms^{-1}) = 0.9355$, assuming last value extrapolation

and,

$\varepsilon_{LW}(T = 288°K, V = 7.5 ms^{-1}) = 0.9708$, assuming emissivity=1 outside data range.

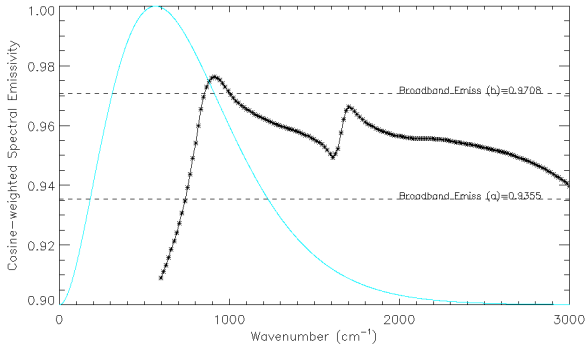

Fig. 3. Convolution of the Planck function with the cosine-weighted emissivity for the non-Lambertian sea surface. The scaled Planck function (cyan) indicates the energy distribution that peaks between 500 to 600 cm^{-1}. The extrapolation method can have a large impact on the convolution result, due to the large portion of energy component in far infrared spectral region, where spectral emissivity is not given. The two assumptions, a) extrapolated with the last given data point, or b) defines emissivity to value one (i.e., as blackbody), produce the broadband emissivity 0.936 and 0.971, respectively.

The non-Lambertian sea surface has a lower broadband emissivity compared to those used in other applications typically range from 0.98 to 1.0, for either extrapolation assumption. Between the two methods, we intend to adapt **0.971**. It is yet to be seen if this broadband emissivity can produce accurate estimate of ULR over the ocean. The validation study will be using the AVHRR-retrieved SST temperature (current NOAA operational algorithm) and ground observations from the CERES Ocean Validation Experiment (COVE) site (http://cove.larc.nasa.gov).

For comparison purpose, the broadband seawater emissivity values derived from different sources are listed in Table 3-4.

Table 3-4. Seawater broadband emissivity for different sources and applications.

SARB Broadband	0.991	Wilbur et al., 1999.
NPOESS	0.991	Assume $\varepsilon(\lambda > 15\mu m) = 1$
CRTM v1.2	0.986, 0.986, 0.982, 0.957	For local zenith angles at 0, 20, 40, 60°, assume $\varepsilon(\nu < 595 cm^{-1}) = 1$
ASTER	0.992	Assume $\varepsilon(\lambda > 14\mu m) = 1$
GSIP	0.985	From NESDIS GSIP implementation. In GSIP ULR calculation, for all surface types, the broadband emissivity is taken from the GOES Imager channel 4 emissivity, based on SeeBor emissivity database (SeeBor et al., 2006)
NCEP GFS	1.000	Non-black emissivity available after May 2007, but GSF model continues to use blackbody assumption due to small changes in net surface LW fluxes. (Yutai Hou, 2007, p.c.)

Deriving Upward Longwave Radiation

The surface upward longwave radiation surface would be the sum of the surface thermal emission plus the reflected flux of the downward longwave radiation. The skin temperature T_{skin} is obtained from the ABI land skin temperature or sea surface temperature retrievals:

$$ULR = \varepsilon_{LW} \cdot \sigma T_{skin}^4 + (1 - \varepsilon_{LW}) \cdot DLR \qquad (3.9)$$

For land, the monthly broadband emissivity climatology is determined from the SeeBor baseline emissivity database, taking surface temperature from the NCEP Reanalysis. For ocean, it is derived from the CRTM seawater emissivity database (CRTM Users Guide). A mean wind speed of 7.5 m/s is assumed for ULR estimation over ocean.

Land, Sea and Coastal

Over the land, the ABI land skin temperature (LST) is used, and over the ocean, the ABI sea surface temperature (SST) is used. Currently, the LST is only retrieved for pixels that are completed covered with land (ie., coastal pixel does not product LST retrievals). The SST is only retrieved over the ocean pixels that are 10 km from the land, but pixels are all filled. The ULR algorithm checks the availability of LST and SST, in order of priority, and if neither is available, missing value is assigned to ULR. Gaps along the coastal lines are therefore expected in the ABI ULR product.

3.4.3 Algorithm Output

3.4.3.1 Output

The algorithm output is the upward longwave radiative flux density at the earth's surface in the unit of Wm^{-2}. The ABI ULR algorithm is performed on pixel level. These pixel values are averaged into the specified horizontal resolution at the product packaging stage. To be consistent with the horizontal resolution of the radiation products, the ULR good quality values are averaged within the required spatial grids (latitude and longitude retangular grid). The spatial resolution of these grids is such that they accommodate the horizontal spatial resolution requirements listed in Table 2-2 with the assumption that one degree in latitude and longitude space equals 100 km. To meet the 60 minute Mode 3 refresh requirement, the ULR product only needs to be run once every hour.

3.4.3.2 Quality Flags

- For ABI ULR algorithm, the QC flags are three two-byte integers:
  - QC_INPUT: 16-bit integer containing input and degradation quality flags
  - QC_RET: 16-bit integer containing retrieval quality flags
- The bit values are defined to start from the least significant bit.
- The QC Flags are diagnostic output on the pixel basis

QC_INPUT: Input

Bit	Quality Flag Name	Meaning	
		zero (default)	one
0	QC_INPUT_LON	Valid Longitude input	Invalid longitude (range check)
1	QC_INPUT_LAT	Valid Latitude input	Invalid latitude (range check)
2	QC_INPUT_LST	Valid LST input	Invalid LST (QC flag check)
3	QC_INPUT_SST	Valid SST input	Invalid SST (QC flag check)
4	QC_INPUT_DLR	Valid DLR input	Invalid DLR (QC flag check)
5	QC_INPUT_EMIS	Valid Emissivity input	Invalid Emissivity input (value -1 is returned from land emissivity reading function)
6	QC_ INPUT _COAST	ULR retrieval is performed not on a coastal pixel	No ULR retrieval because of coastal pixel
7	QC_ INPUT _DLR	ULR retrieval uses valid DLR	DLR is not available. ULR is retrieved using unity emissivity assumption
8	QC_ INPUT _EMIS	ULR retrieval uses valid Emissivity	Emissivity is not available. ULR is retrieved using unity emissivity assumption

9			
10			
11			
12			
13			
14			
15			

QC_RET: Success/failure of retrieval

Bit	Quality Flag Name	Meaning	
		zero (default)	one
0	QC_RET_OVERALL	Overall success of retrieval	Overall failure of retrieval
1	QC_RET_INPUT	Valid input parameters	Retrieval failed due to invalid input
2	QC_RET_OUTPUT	Valid ULR output	Retrieval failed due to invalid ULR output (out of range)
3			
4			
5			
6			
7			

3.4.3.3 Metadata

These Metadata provide quick tracking of product properties over the respective domains. They are derived for each hourly map.

Conus Product

Name	Description	Data Type	
META_ULR_CN_MEAN	Mean ULR over Conus domain	Real*4	
META_ULR_CN_STD	Standard deviation of ULR over Conus	Real*4	
META_ULR_CN_MAX	Maximum ULR over Conus	Real*4	
META_ULR_CN_MIN	Minimum ULR over Conus	Real*4	
META_ULR_CN_VALID	Percentage of ULR with each QA flag value	Real*4	

Full Disc Product

Name	Description	Data Type	
META_ULR_FD_MEAN	Mean ULR over FD domain	Real*4	
META_ULR_FD_STD	Standard deviation of ULR over FD	Real*4	
META_ULR_FD_MAX	Maximum ULR over FD	Real*4	
META_ULR_FD_MIN	Minimum ULR over FD	Real*4	
META_ULR_FD_VALID	Percentage of ULR with each QA flag value	Real*4	

3.4.3.4 Diagnostic Output

The parameters defined here are the diagnostic output that will be generated for product validation and verification purposes.

For each of the output grid boxes at the product output resolution:

Name	Description	Data Type	Dimension
NUM_ULR_RET	Number of successful ULR retrievals at pixel level	Integer*2	grid (xsize, ysize)
STD_ULR_RET	Standard deviation of ULR retrievals	Real*4	grid (xsize, ysize)

* Grid (xsize and ysize) are the output grid dimension that is product specific and is determined by the post processing.

4 TEST DATA SETS AND OUTPUTS

4.1 Simulated/Proxy Input Data Sets

The ABI ULR algorithm is evaluated using the GOES Sounder and Imager skin temperature retrievals over both the land and the ocean. These retrievals have close proximity to the future ABI algorithms. The AWG LST Team (Yunyue Bob Yu) provides one year worth of land skin temperature retrievals from the ABI candidate algorithm using GOES Imager observations. The AWG SST Team (Alexander Ignatov) provides ocean surface (skin) temperature retrievals from a SST heritage algorithm using AVHRR observations.

Land

The AWG LST team recommends the Prata & Platt (1991) and Caseeles et al. (1997) skin temperature algorithm for the ABI (Bob Yu, pers. comm., Jan 2008). We validated the ULR with SURFRAD ground observations using the skin temperatures from GOES Imager observations with that algorithm. Skin temperature retrieval is only available in clear-sky condition. We also tested with the skin temperature from the operational GOES sounder retrieval system.

Temporal matching issue

Current GOES Imager temporal matching is set at a constant lag of 5 minutes from the beginning of the scans. This estimation produces errors in the overpassing time that may result in ULR biases. Better temporal matched validation data set will be available in the near future and the results will be updated.

Ocean

The operational AVHRR sea surface temperature retrieval product is used to assess the ULR retrieval over ocean. The surface validation reference source is obtained from the CERES Ocean Validation Experiment (COVE) measurement.

4.2 Output from Simulated/Proxy Inputs Data Sets

Land

When the LW surface emissivity and the downward longwave radiation are known, the total ULR is calculated as the surface thermal emission plus the reflected downward thermal radiation (assuming negligent transmission). When the emissivity information or the downward longwave radiation is not known, we need to estimate an "effective emissivity", which is a broadband emissivity that will produce the equivalent total upward thermal radiation including the reflected radiation (see Eq. 3.6). For error assessment purpose, we compared the ULR from

a) **Grey body emissivity,** surrogated by the window channel emissivity used in the land skin temperature retrieval
b) **Effective emissivity** at value one (namely, assuming blackbody).

These two approaches served as the limiting cases and their results are shown in Table 4-1. Table 4-2 summarizes the GOES Sounder retrieval validation results. Overestimation at high end of ULR using the constant effective emissivity is more noticeable (see Fig. 2).

Table 4-1. Statistics for GOES Imager ULR validation results from all sites.

	Mean Diff Wm^{-2}	**STD Diff Wm^{-2}**	**RMS Diff Wm^{-2}**	**Corr. Coef.**	**Number of cases**	**Period**
Grey body emissivity	-2.8	10.5	10.9	0.993	20,027	2001
Effective emissivity (=1.)	0.2	11.1	11.1	0.992	20,027	2001

Table 4-2. Statistics for GOES Sounder ULR validation results from all sites.

	Mean Diff Wm^{-2}	**STD Diff Wm^{-2}**	**RMS Diff Wm^{-2}**	**Corr. Coef.**	**Number of cases**	**Period**
Effective emissivity (=1.)	-1.4	16.1	16.2	0.943	1400	2008.1.1-2008.4.4

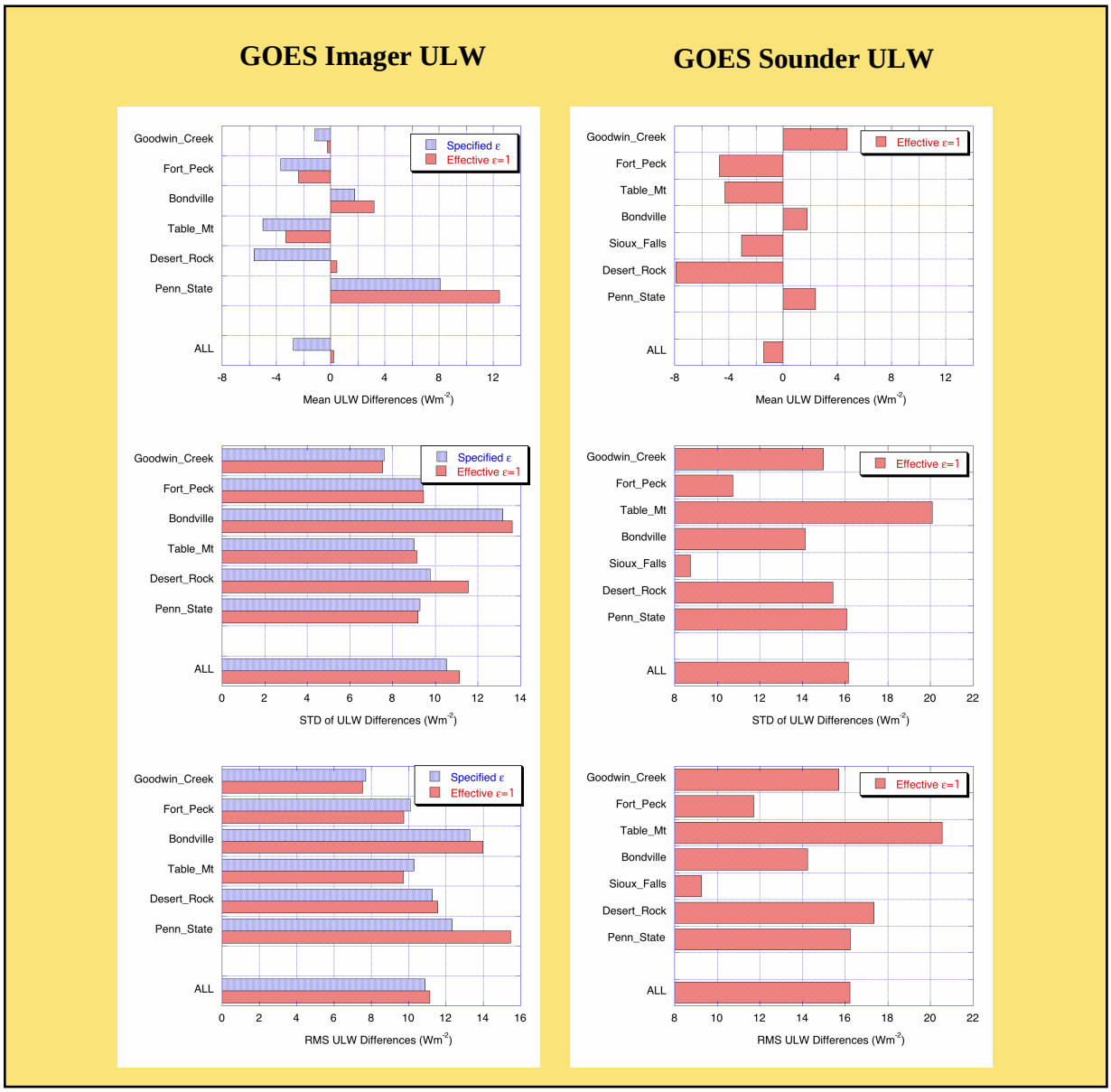

Figure 4-1 Validation statistics for ULW estimated using GOES Imager and Sounder skin temperature retrievals compared to the Precision Infrared Radiometer (PIR) ground observations at seven NOAA SURFRAD stations.

The Imager data were from year 2001; the 3-month sounder data were from Jan 1 to April 4, 2008. The skin temperature was retrieved only for clear sky condition. Various quality control procedures were placed to eliminate cloud-contaminated scenes. The Imager ULW were derived in two ways by a) using specified grey body emissivity and, b) assuming a constant effective broadband emissivity of 1.

While the mean ULW differences from the two observing/retrieval systems are comparable, averaged to within about 2 Wm^{-2}, the standard deviation of ULW differences for the Sounder ULW differences are about 5 Wm^{-2} larger than that of the Imager. There are intrinsic differences in the retrieval methods for these two instruments. The fact that the Imager data were further handpicked for clear scene might be partially responsible for better agreement.

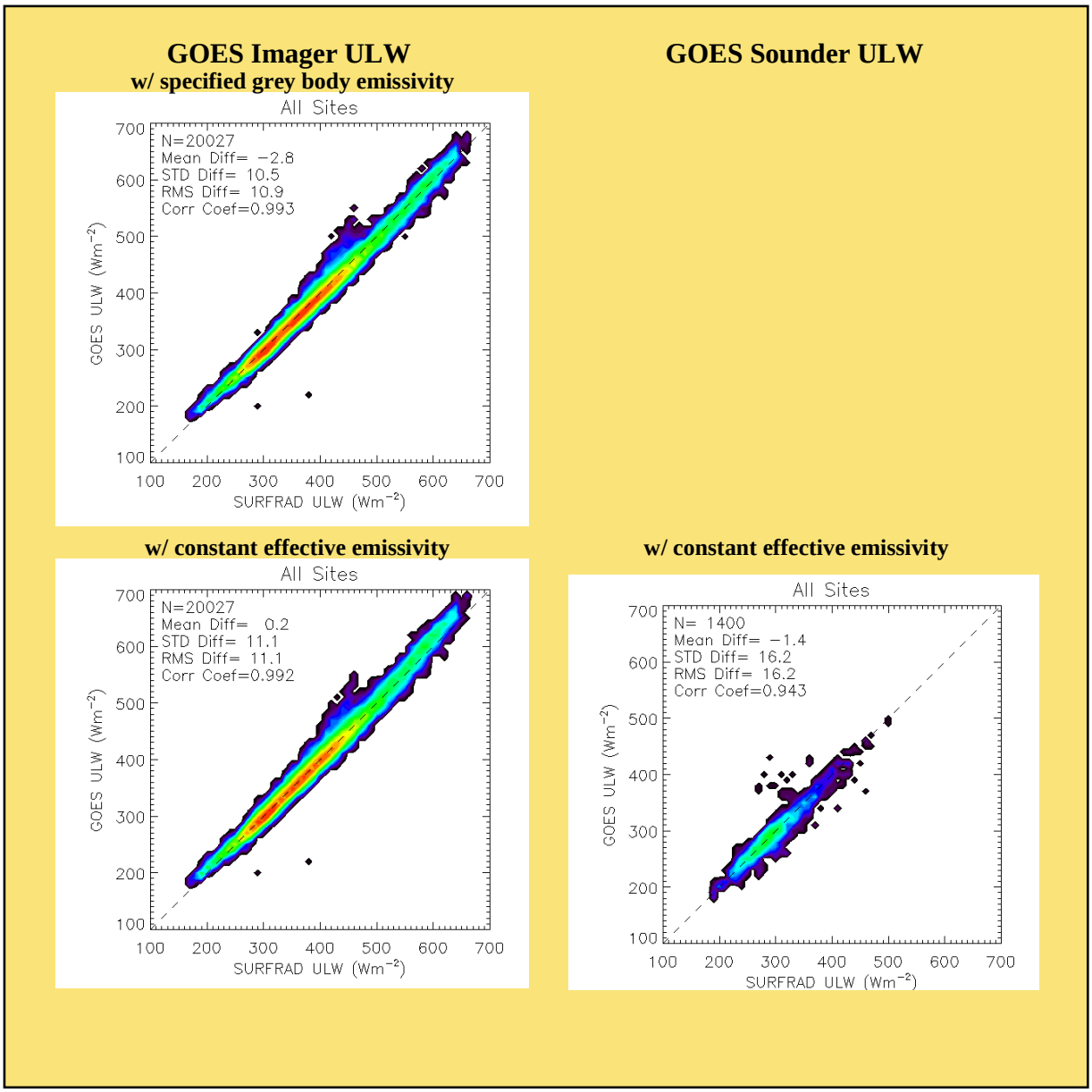

Figure 4-2 GOES Imager and Sounder derived ULW compared to the Precision Infrared Radiometer (PIR) ground observations from all NOAA SURFRAD stations.

The Imager ULW were derived in two ways by a) using specified grey body emissivity (left top) and, b) assuming a constant effective broadband emissivity of 1 (left bottom). The Sounder ULW was derived with a constant effective broadband emissivity of 1 (right bottom).

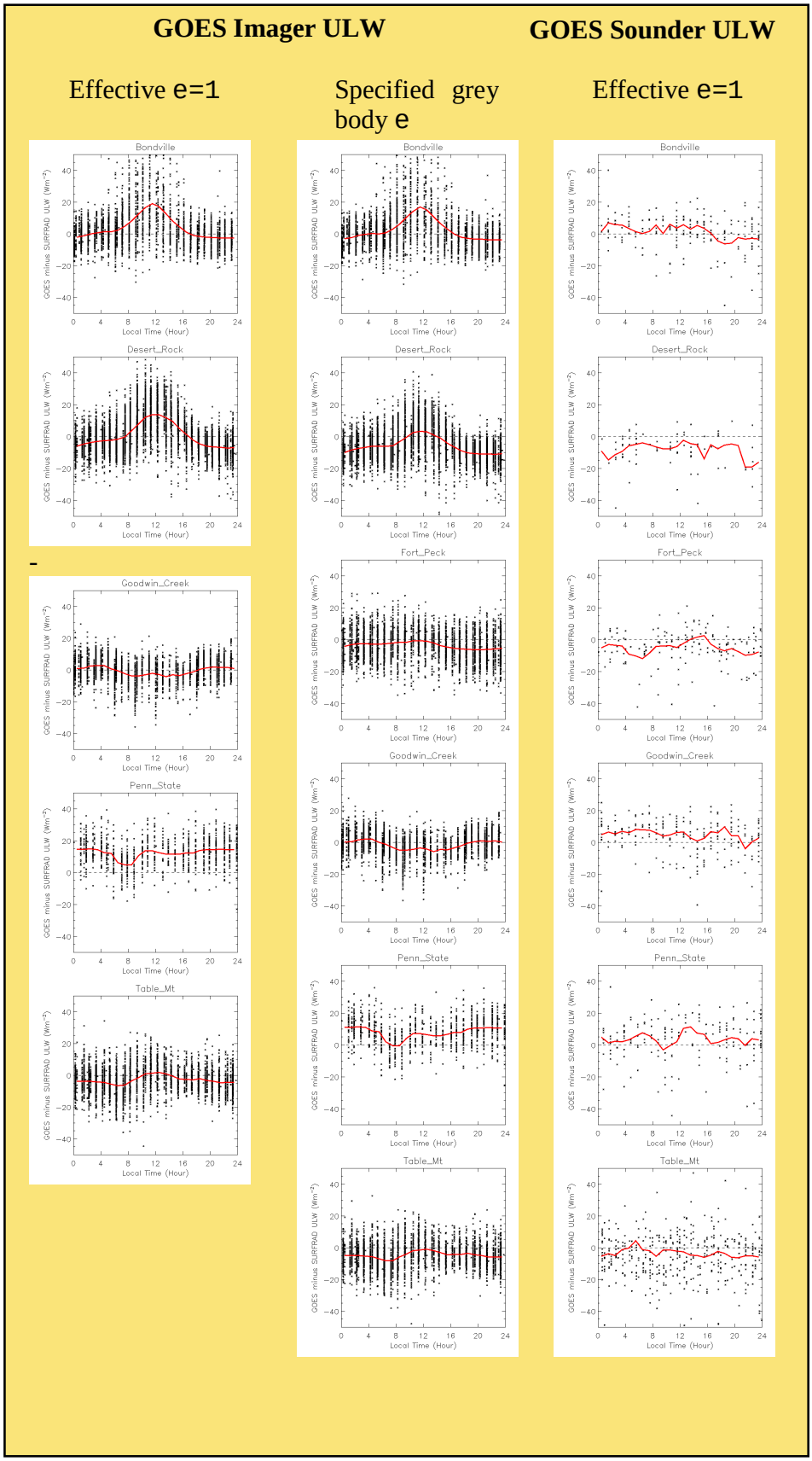

Figure 4-3 Examination of the diurnal dependency in ULW retrieval errors.

The ULW differences are plotted as functions of local time for six SURFRAD stations: Bondville, Desert Rock, Fort Peck, Goodwin Creek, Penn Stat, and Table Mountain from top to bottom. The three columns correspond to the ULW estimated from GOES Imager using a constant effective emissivity of one, GOES Imager using the specific grey body emissivity, and GOES Sounder using a constant effective emissivity of one, respectively.

The diurnal dependent errors in GOES Imager ULW were reduced after a software bug in temporal matching was corrected. However, the scanning times are still not exactly correct for each station, as a fix 5 minutes lag is currently employed. The Bondville and Desert Rock showed the strongest diurnal pattern in ULW errors with noontime over estimations.

The GOES Sounder ULW did not show errors with apparent diurnal dependency. But this might be due to the limited season sampling (only 3 months of data) that this test may not cover the full range of ULW variability.

Ocean
The validation results are not available yet. However, since the oceanic scene is considered more homogeneous with relatively stable emissivity, the magnitude of errors in ULR over the ocean would be smaller than those from the land sites.

4.2.1 Accuracy and Precisions of Estimates

Table 4-3 summaries the estimated accuracy and precision for the ABI ULR algorithm assessed with the one year worth of GOES Imager LST retrievals compared to the SURFRAD ground observations. These results indicate that the ULR product meets the F&PS 100% requirement.

Table 4-3. Accuracy and precisions requirement and assessments from current validation studies.

	F&PS			**Algorithm Evaluation**		
Wm^{-2}	Accuracy	Precision	Range	Accuracy	Precision	
ULR	30	20	50-900	3	11	Offline[(1)]

[(1)] Offline land cases.

4.2.2 Error Budget

The errors in ULR are contributed from these components:

$$\Delta ULR = \varepsilon \cdot 4\sigma T_s^3 \Delta T_s + \Delta\varepsilon \cdot \sigma T_s^4 + \Delta\varepsilon \cdot DLR + (1-\varepsilon)\Delta DLR \qquad (4.1)$$

The primary error source for ULR retrieval is in the estimation of the surface temperature.

According to F&PS, the accuracy requirement for land skin temperature is 4.8°C and land (window) surface emissivity is 0.05. Assuming that the broadband emissivity is also accurate to ±0.05, and assuming that the two error sources are independent (this is not necessarily true because the temperature and emissivity could be simultaneously retrieved), and assuming DLR at 250 Wm^{-2}, the magnitude of bias of ULR would be bound by

$$\Delta ULR = \sqrt{\left(\varepsilon \cdot 4\sigma T_s^3 \Delta T_s\right)^2 + \left(\Delta\varepsilon \cdot \sigma T_s^4\right)^2 + \left(\Delta\varepsilon \cdot DLR\right)^2} \qquad (4.2)$$

Assume Ts=288°K, emissivity at 1, the ULR error would be about 35 Wm^{-2}, given the temperature error at 4.8°C. The land skin temperature estimation would be accurate to 2.5°C with known emissivity, known atmospheric correction and 80% channel correlations, the ULR error would be reduced to about 14 Wm^{-2}. The F&PS accuracy

requirement of 30 Wm^{-2} is a reasonable estimate of achievable accuracy given these conditions.

Unit Test Readiness Results

The development and tests are performed on orbit199l.orbit2.nesdis.noaa.gov – Linux (2.33GHz 2 dual core CPUs with 2 GB memory/CPU, 2TB disk space). The machine is physically located at NOAA/NESDIS/STAR within the STAR collaborative environment and maintained by STAR IT.

A sample data set containing 200 cases has been used in the Framework Software Readiness Test. The input variables include the month, latitude, longitude, surface/skin temperature and the static monthly emissivity maps. The reference ULR flux data provided is derived from the offline system at CICS. The resulting ULR Flux values are exactly the same as the offline results – Zero pixels differ.

5 PRACTICAL CONSIDERATIONS

5.1 Numerical Computation Considerations

ULR retrieval is performed on the pixel basis, independent from other pixels. This is ideal for vector processing. Although the flow chart is now designed for pixel processing, it would be more efficient to extend it to one scan unit, or the next larger processing unit, e.g., a granule.

5.2 Programming and Procedural Considerations

The ULR is a pixel-by-pixel algorithm. It does not use ABI radiance measurement directly. Its ancillary inputs include skin temperature, window emissivity, and downward longwave radiation. It should be placed at the end of the Earth radiation budget production modules that are near the end of the production chain.

5.3 Quality Assessment and Diagnostics

Describe how the quality of the output products and the retrieval itself is assessed, documented, and any anomalies diagnosed. This is designed for real time or near real time processing.

The following procedures are recommended for diagnosing the performance of the ULR.

- Routine/Operational Product Evaluation and Monitoring are necessary.
- Automatic analysis/statistics generated for collocated ABI and reference sources, including:
- SURFRAD (near real time)
- ARM (near real time)
- CERES SARB (not available in real time)
- NWP surface analysis (LDAS and SST)
- QA Metrics/Flags to be defined.

5.4 Exception Handling

The ULR module will check validity of the ancillary input data if flags were provided. The valid range of ULR will also be checked. The missing value will be assigned when calculation results are outside the allowed range or the algorithm does not lead to a valid derivation.

5.5 Algorithm Validation

The validation reference data source are from the ground observation networks, including the NOAA Surface Radiation network (SURFRAD) and the DOE Atmospheric Radiation Measurement (ARM) network. These ground stations provide upward longwave radiative flux measurement at a very high frequency that typically 3 minutes average data is used for our validation purpose. The satellite estimated ULR will be compared against the concurrent ground observations at certain collocation requirement to yield proper representations of the product accuracy, considering the spatial differences of these two observing methods. As the product is clear sky only, the effectiveness of cloud filtering becomes a source of error. The availability of the ground observations is about 1 day lag, so the product quality assessment and monitoring is best performed at the near-real time frame.

6 ASSUMPTIONS AND LIMITATIONS

The following sections describe the current limitations and assumptions in the current version of the ULR.

6.1 Performance

The ABI ULR algorithm is mainly evaluated using a surrogate algorithm tested with the GOES Imager and Sounder observations. The evaluation of ABI ULR algorithm is possible when quality simulation data is available. The broadband emissivity is not yet available. The grey body and effective emissivity assumptions were evaluated as the limiting cases.

The retrieval performance assessed with algorithm should be within that of the ABI ULR algorithm. Further improvements can be made when broadband emissivity and reflectivity are accurately estimated. The diurnal dependence in ULR errors is not fully understood yet. The static emissivity map used in CERES SARB production (Wilber et al., 1999) is the fallback emissivity data source.

6.1.1 Graceful Degradation

The ULR calculation requires the surface temperature that is provided from AWG LST or SST retrievals. Since there has no LST retrievals on coastal pixels and there has no SST retrievals within 10 km of land, there will be gaps in the ULR products along the coastal line. Currently we do not have alternative input source for the surface temperature, the ULR will be assigned missing in such cases. The ABI sounding retrieves surface temperature (as a intermediate product) that can be considered as the alternative input. Currently, this is not implemented.

6.2 Assumed Sensor Performance

The ULR derivation involves retrieval products and the broadband emissivity and reflectivity determination. The sensor biases/noises can affect the ULR quality through the retrieval products, mainly the skin temperature and window emissivity, but its magnitude cannot be estimated directly.

6.3 Pre-Planned Product Improvements

The overall performance of the ABI ULR algorithm is marginally satisfactory. The error sources include the skin temperature retrieval as well the uncertainties in prescribing the emissivity. The use of broadband emissivity and reflectivity determined from the given window emissivity retrievals and atmospheric states may improve the ULR calculation, expectedly to reduce the bias errors. The ULR diurnal-dependent error also requires further investigation.

Studies using ABI simulation data would be very useful in pre-launch testing.

6.3.1 Improvement 1

Collaborating with the LST/SST algorithm teams to investigate the diurnally dependent bias. The noontime over estimation of ULR is likely a result of over estimation of the land surface temperature and that is under investigation.

6.3.2 Improvement 2

Use ABI simulated radiance to derive surface temperature for ULR determination. This would produce more precise assessment of the ABI ULR product accuracy and precision.

6.3.3 Improvement 3

Update broadband longwave emissivity climatology when SeeBor emissivity database is updated.

6.3.4 Improvement 4

Investigate the feasibility of deriving dynamical broadband emissivity using ABI derived window emissivity (an option-2 product) along with the SeeBor emissivity database. This will further reduce the bias error associated with the emissivity estimation.

7 REFERENCES

ASTER Spectra Library: http://speclib.jpl.nasa.gov (as of Aug 13, 2008)

Baldridge, A.M., S.J. Hook, C.I. Grove, G. Rivera, 2009: The ASTER Spectral Library Version 2.0. http://speclib.jpl.nasa.gov/downloads/RSE_D_08_00553.pdf

CERES Ocean Validation Experiment: http://cove.larc.nasa.gov/

CERES ATBD Subsystem 5.0 release 2.2, 1997: Compute Surface and Atmospheric Fluxes (http://science.larc.nasa.gov/ceres/ATBD/pdf/ceres-atbd2.2-s5.0.pdf)

Caselles, V., C. Coll and E. Valor, 1997: Land surface temperature determination in the whole Hapex Sahell area from AVHRR data. Int. J. remote Sens. 18, 5, 1009-1027, 1997.

CRTM v1.2 User Guide, 2009: ftp://ftp.emc.ncep.noaa.gov

Jin, M. and S. Liang, 2006: An improved land surface emissivity parameter for land surface models using global remote sensing observations. J. Climate, 19, 2861-2887

Ogawa, K.; Schmugge, T.; Jacob, F.; French, A., 2002: Estimation of broadband emissivity from satellite multi-channel thermal infrared data using spectral libraries Geoscience and Remote Sensing Symposium, IGARSS apos;02. 2002 *IEEE International,* **6**, 3234 – 3236. 10.1109/IGARSS.2002.1027140

Prata, A. J. and C.M.R. Platt, 1991: Land surface temperature measurements from the AVHRR. Proc. of the 5th AVHRR Data users conference, June 25-28, Tromso, Norway, EUM P09, 443-438, 1991.

Salisbury, J. W. and D. M. D'Aria, 1992: Emissivity of terrestrial materials in the 8–14 μm atmospheric window. *Remote Sens. Environ.,* **42**, 83-106.

Seemann, S.W., E. E. Borbas, R. O. Knuteson, G. R. Stephenson, H.-L. Huang, 2008: Development of a global infrared land surface emissivity database for application to clear sky sounding retrievals from multi-spectral satellite radiance measurements. *J. Appl. Meteor. Climatol.*, **47**, 108-123

van Delst, P.F.W. and Wu, X., 2000: A high resolution infrared sea surface emissivity database for satellite applications. Technical Proceedings of The Eleventh International ATOVS Study Conference, Budapest, Hungary 20-26 September 2000, 407-411

Wang, K., Z. Wan, P. Wang, M. Sparrow, J. Liu, X. Zhou, and S. Haginoya, 2005: Estimation of surface long wave radiation and broadband emissivity using Moderate Resolution Imaging Spectroradiometer (MODIS) land surface temperature/emissivity products. *J.G.R.*, **110,** D11109, doi:10.1029/2004JD005566.

Wilber, A., D. Kratz, and S. Gupta, 1999: Surface Emissivity Maps for Use in Satellite Retrievals of Longwave Radiation. NASA/TP-1999-209362

Yu, Yunyue, D. Tarpley, M.K. R. V. Raja, H. Xu, K. Vinnikov, 2008: Applying Split Window Technique for Land Surface Temperature Measurement from GOES-R Advanced Baseline Imager. GOES-R Users Conferences, Jan 22-24, 2008, New Orleans, LA.

Appendix 1: Common Ancillary Data Sets

1. SFC_EMISS_SEEBOR

a. *Data description*

Description: Surface emissivity at 5km resolution
Filename: global_emiss_intABI_YYYYDDD.nc

Where, YYYYDDD = year plus Julian day
Origin: UW Baseline Fit, Seeman and Borbas (2006).
Size: 693 MB x 12
Static/Dynamic: Dynamic

b. *Interpolation description*

The closest point is used for each satellite pixel:

1) Given ancillary grid of large size than satellite grid
2) In Latitude / Longitude space, use the ancillary data closest to the satellite pixel.

2. NWP_GFS

a. *Data description*

Description: NCEP GFS model data in grib format – 1 x 1 degree (360x181), 26 levels
Filename: gfs.tHHz.pgrbfhh
Where,
HH – Forecast time in hour: 00, 06, 12, 18
hh – Previous hours used to make forecast: 00, 03, 06, 09
Origin: NCEP
Size: 26MB
Static/Dynamic: Dynamic

b. Interpolation description

There are three interpolations are installed:

NWP forecast interpolation from different forecast time:

Load two NWP grib files which are for two different forecast time and interpolate to the satellite time using linear interpolation with time difference.

Suppose:

T1, T2 are NWP forecast time, T is satellite observation time, and T1 < T < T2. Y is any NWP field. Then field Y at satellite observation time T is:

$$Y(T) = Y(T1) * W(T1) + Y(T2) * W(T2)$$

Where W is weight and

$$W(T1) = 1 – (T-T1) / (T2-T1)$$
$$W(T2) = (T-T1) / (T2-T1)$$

NWP forecast spatial interpolation from NWP forecast grid points. This interpolation generates the NWP forecast for the satellite pixel from the NWP forecast grid dataset.

The closest point is used for each satellite pixel:

1) Given NWP forecast grid of large size than satellite grid
2) In Latitude / Longitude space, use the ancillary data closest to the satellite pixel.

NWP forecast profile vertical interpolation

Interpolate NWP GFS profile from 26 pressure levels to 101 pressure levels

For vertical profile interpolation, linear interpolation with Log pressure is used:

Suppose:

y is temperature or water vapor at 26 levels, and y101 is temperature or water vapor at 101 levels. p is any pressure level between p(i) and p(i-1), with p(i-1) < p <p(i). y(i) and y(i-1) are y at pressure level p(i) and p(i-1). Then y101 at pressure p level is:

$$y101(p) = y(i-1) + \log(p[i] / p[i-1]) * (y[i] – y[i-1]) / \log (p[i] / p[i-1])$$